Available online at www.sciencedirect.com
SCIENCE DIRECT®

Journal of the European Ceramic Society 24 (2004) 2641–2648

www.elsevier.com/locate/jeurceramsoc

Preparation and characterization of dense $Ce_{0.85}Y_{0.15}O_{2-\delta}$ ceramics

J. Ma[a], T.S. Zhang[a,*], L.B. Kong[a], P. Hing[a], Y.J. Leng[b], S.H. Chan[b]

[a]*School of Materials Engineering, Nanyang Technological University, Nanyang Avenue, Singapore 639798*
[b]*School of Mechanical and Production Engineering, Nanyang Technological University, Nanyang Avenue, Singapore 639798*

Received 12 June 2003; received in revised form 18 September 2003; accepted 27 September 2003

Abstract

The precursor powder of $Ce_{0.85}Y_{0.15}O_{2-\delta}$ has been prepared via oxalate coprecipitation from high purity reagents of $Ce(NO_3)_3{\cdot}6H_2O$ and $Y(NO_3)_3{\cdot}6H_2O$. The sinterability, densification and microstructural development have been examined. At all the sintering temperatures used from 1000 to 1550 °C, no intragranular pores are observed. All the pores are located at the grain boundaries or at the triple points. The sample sintered at 1300 °C for 3 h has over 98.0% relative density, and a mean grain size of ~1.55 μm. Nearly all the pores are eliminated from the sintered bodies, when the sintering temperature is higher than 1300 °C. Higher ionic conductivity [e.g., 4.59 $(\Omega m)^{-1}$ at 750 °C in air] is obtained for the $Ce_{0.85}Y_{0.15}O_{2-\delta}$ ceramic sintered at 1300 °C in 3 h. This sample has a fracture toughness of 1.49 ± 0.2 MPa $m^{1/2}$. However, no fracture toughness dependence of grain size is found for dense $Ce_{0.85}Y_{0.15}O_{2-\delta}$ ceramics.

Keywords: CeO_2; Ionic conductivity; Mechanical properties; Y_2O_3

1. Introduction

Yttria-stabilized zirconia (YSZ) is traditionally used as an electrolyte material of solid oxide fuel cell (SOFC) because of its relatively high ionic conductivity, high stability under oxidizing and reducing atmospheres at high temperatures. YSZ electrolyte is generally operated at about 1000 °C, where the ionic conductivity reaches the required high level. However, such high temperatures often lead to reactions between the components, thermal degradation, or thermal expansion mismatch. Moreover, cell interconnectors and seals have to be selected to meet severe limitations of high operation temperature.

Recently, an intensive investigation has been done to reduce the operating temperature of SOFC down to 800–500 °C. Ceria-based solid solutions have been regarded as the most promising electrolytes for intermediate temperature SOFC (IT-SOFC) because of their ionic conductivity is higher than YSZ. The ionic conductivity of ceria has been extensively investigated with respect to different dopants (e.g., Ca^{2+}, Sr^{2+}, Y^{3+}, La^{3+}, Gd^{3+}, and Sm^{3+}) and dopant concentration.[1–4] It is generally accepted that Gd^{3+} or Sm^{3+}-doped ceria exhibits the highest conductivity due to the small association enthalpy between dopant cation and oxygen vacancy in the fluorite lattice.[5,6] However, carefully examining literature data as listed in Table 1, it seems that the above conclusion is not so convincing because the conductivity of Y-doped ceria ceramics can compare well with those reported for Gd- or Sm-doped ceria ceramics. Moreover, compared with the Gd-doped ceria ceramics, Y-doped ceria ceramics exhibit less aging behavior, which will be reported in another communication.[16] Therefore, Y-doped ceria is also potentially one of promising electrolytes for IT-SOFCs.

It is well known that as refractory materials, ceria-based ceramics are difficult to densify below 1500 °C. In order to reduce sintering temperatures, various aqueous-solution based precipitation systems have been exploited for preparing nanocrystalline ceria-based powders, including precipitation using ammonia,[17] ammonium carbonate,[18] hydrazine hydrate,[19] oxalic acid precipitant,[11,20] forced hydrolysis of inorganic salts,[21] urea-based homogeneous precipitation,[22] and hexamethylenetetramine (HMT)-based homogeneous precipitation.[23] Among these precipitation systems,

* Corresponding author. Fax: +65-6790-0920.
E-mail address: tszhang@ntu.edu.sg (T.S. Zhang).

0955-2219/$ - see front matter © 2003 Elsevier Ltd. All rights reserved.
doi:10.1016/j.jeurceramsoc.2003.09.023

Table 1
Selected literature data regarding the ionic conductivity at 750 °C in air of ceria-based solid solutions

Compound	σ $(\Omega m)^{-1}$	Ref.
$Ce_{0.8}Y_{0.2}O_{2-\delta}$	1.9	7
$Ce_{0.85}Y_{0.15}O_{2-\delta}$	2.0	8
$Ce_{0.82}Y_{0.18}O_{2-\delta}$	4.0	9
$Ce_{0.8}Y_{0.2}O_{2-\delta}$	5.5	10
$Ce_{0.8}Y_{0.2}O_{2-\delta}$	6.5	11
$Ce_{0.82}Gd_{0.18}O_{2-\delta}$	2.6	7
$Ce_{0.8}Gd_{0.2}O_{2-\delta}$	3.3	12
$Ce_{0.8}Gd_{0.2}O_{2-\delta}$	5.68	13
$Ce_{0.9}Gd_{0.1}O_{2-\delta}$	5.9	14
$Ce_{0.8}Gd_{0.2}O_{2-\delta}$	6.5	15
$Ce_{0.8}Sm_{0.2}O_{2-\delta}$	3.1	7
$Ce_{0.82}Sm_{0.18}O_{2-\delta}$	4.0	4
$Ce_{0.8}Sm_{0.2}O_{2-\delta}$	6.1	12
$Ce_{0.8}Sm_{0.2}O_{2-\delta}$	6.9	10

oxalate precipitation and HMT-based homogeneous precipitation are most useful for obtaining better ceria-based powders.

In this study, ultrafine powder of $Ce_{0.85}Y_{0.15}O_{2-\delta}$ has been prepared via an oxalate coprecipitation process. The sinterability, densification, and microstructural development have been examined. Moreover, the electrical and mechanical properties of dense $Ce_{0.85}Y_{0.15}O_{2-\delta}$ ceramics have also been investigated and presented.

2. Experimental procedure

2.1. Preparation of raw powders

An oxalate coprecipitation method was used to prepare the precursor powders of $Ce_{0.85}Y_{0.15}O_{2-\delta}$ ceramics. High purity (>99.5%) reagents $Ce(NO_3)_3{\cdot}6H_2O$ and $Y(NO_3)_3{\cdot}6H_2O$ were used as starting materials. Oxalic acid solution was used as a coprecipitation medium. The preparation procedure used in this research is similar to that reported by Higashi et al.[20] It involves: (1) $Ce(NO_3)_3{\cdot}6H_2O$ and $Y(NO_3)_3{\cdot}6H_2O$ were dissolved in distilled water, respectively. A mixture of Y^{3+} and Ce^{3+} ions were prepared by blending the above two solutions. (2) The mixture was added into the oxalic acid solution at ~60 °C. During this process, the precipitant solution was controlled at pH = 6.5–7 by dropwise addition of diluted ammonia, and was stirred constantly. After the coprecipitation was completed, the coprecipitate was stirred at ~60 °C for 1 h. (3) The coprecipitate was washed several times using distilled water, then redispersed and washed twice in ethanol, finally dried at ~100 °C for 20 h.

2.2. Characterization of samples

Thermal gravimetric-differential thermal analysis (TG-DTA) was conducted for the coprecipitated powders with a heating rate of 5 °C min^{-1} up to 1000 °C in air. The crystal structure of the calcined samples was analyzed using X-ray diffraction (XRD) with CuK_a radiation. Specific surface area was estimated by BET (Brunauer–Emmett–Teller) method using nitrogen as the absorption gas. The morphology of particles was observed under scanning electron microscopy (SEM).

The coprecipitated powder was calcined at 400–900 °C for 3 h, then ground in ethanol via a planetary milling system using polypropylene jars with yttria-stabilized zirconia balls for 8 h. The calcined powder was pressed at ~200 MPa into pellets using a die 10 mm diameter. The pellets were sintered at the temperature range of 1000–1550 °C for 3 h. The densities of green and sintered pellets were calculated from the mass and dimension of the samples, and measured using Archimedes method with water, respectively. The microstructure of the sintered samples (i.e., well-polished surface after thermal etching) was observed using SEM, and grain size was calculated from SEM micrographs using the linear intercept technique.

Silver wires were used as the electrodes and silver paste at 850 °C was used to fix silver wire onto both sides of the sintered pellets. Ionic conductivity of the samples was measured from 250 to 850 °C in air by two-probe impedance spectroscopy (Solartron 1260, UK) in the frequency range of 1–10^7 Hz. A software package was also used to separate the grain interior (GI) and the grain boundary (GB) contributions to the total conductivity.

Sintered pellets were polished on one face using 1 μm diamond paste before indentation testing. Vickers hardness was measured using a microhardness tester (HSV-20, Shimadzu, Japan) with the load range of 2–100 N, and held for 30 s. At least 10 indentations were used for obtaining the average values of hardness and fracture toughness.

3. Results and discussion

3.1. Powder characterization

Similar to the previous work,[18] our TG-DTA results as shown in Fig. 1 indicate that at ~175 °C, the coprecipitated powder loses chemically adsorbed water, and decomposes to oxides at ~325 °C; no remarkable changes can be detected above 350 °C in both TG and DTA curves. The sample calcined at 400 °C shows a very broaden XRD peak at $2\theta = \sim 29^\circ$, indicating that this sample has low crystallinity. However, when the calcination temperature is around 600 °C or above, the

crystalline phase is well-developed. The effect of calcination on powder characteristics has been studied and the results are listed in Table 2. The mean crystallite size (R_x) is determined using X-ray line broadening method:[24]

$$R_x = 0.9\lambda/(\beta\cos\theta) \quad (1)$$

where λ is the wavelength of the incident X-ray (0.15406 nm); θ is the diffraction angle; and β is the corrected half-width. For the green bodies calcined at 400–900 °C, which can be treated as the mixture of two distinct phases of CeO_2 and Y_2O_3, the theoretical density is:[25]

$$\boldsymbol{d}_{\mathrm{th}}^{G} = \frac{d_{CeO_2}\left(1+\frac{C}{1-C}\frac{M_{Y_2O_3}}{M_{CeO_2}}\right)}{\left(1+\frac{C}{1-C}\frac{d_{CeO_2}}{d_{Y_2O_3}}\frac{M_{Y_2O_3}}{M_{CeO_2}}\right)} \quad (2)$$

where $C = x/(2-x)$ and $x = 0.15$ in the present study; $\boldsymbol{d}_{CeO_2} = 7.22$ g/cm^3 and $\boldsymbol{d}_{Y_2O_3} = 5.03$ g/cm^3; M is molecular weight. We get $\boldsymbol{d}_{\mathrm{th}}^{G} = 6.91$ g/cm^3 for the mixture of 0.85 CeO_2 + 0.15 $YO_{1.5}$ (i.e., $x = 0.15$) according to Eq. (2).

The morphology of the powder calcined at 700 °C for 3 h is shown in Fig. 2. It clearly shows that the powder consists of agglomerated nanocrystallites. It is generally accepted that the densification behavior and final density depend significantly on the state of agglomeration in powders. The soft agglomerates pack uniformly, resulting in homogeneous shrinkage of powder compacts to near-theoretical density. The hard agglomerates during sintering pull away from the surrounding regions and leave large pores since they densify first, which prevents complete densification. It is difficult to avoid the formation of hard agglomeration in powders prepared by wet chemical means. However, the extent of agglomerates significantly relays on the preparation method and washing medium. In this study, the coprecipitated precursor of Y-doped CeO_2 was redispersed and washed twice in ethanol. This is an important step for obtaining a better precursor powder.

3.2. Sintering behavior and microstructure

Calcination temperature has a significant effect on powder characteristics as listed in Table 2. It also affects the densification behavior of $Ce_{0.85}Y_{0.15}O_{2-\delta}$ ceramics. In this study, 700 °C is chosen as calcination temperature because higher sintered density can be obtained for the samples prepared from the powder calcined at 700 °C in 3 h. The sintered samples are expected to form solid solution where Y^{3+} ions occupy Ce^{4+} sites. The theoretical density is then:[25]

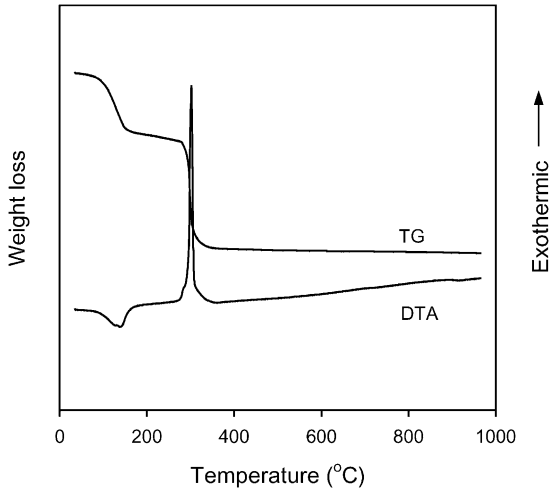

Fig. 1. TG–DTA curves of the coprecipitated powder conducted at a heating rate of 5 °C/min to 1000 °C in air.

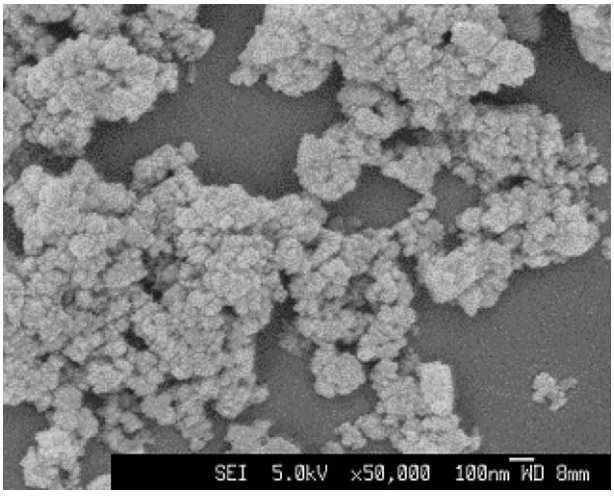

Fig. 2. The morphology of the powder calcined at 700 °C for 3 h in air.

Table 2
The effect of calcination on the powder characteristics

Calcination temperature (°C)	400	500	600	700	800	900
BET surface area (m^2/g)	82.5	72.3	50.1	24.5	16.7	7.6
Crystallite size, R_x (nm)	6.5	7.2	11.25	16.3	28	45
Green density[a] (%)	38.6	39.2	44.5	47.6	50.3	54.5

[a] The relative density of green bodies is calculated using the theoretical density of 6.91 g/cm^3 that is obtained from Eq. (2).

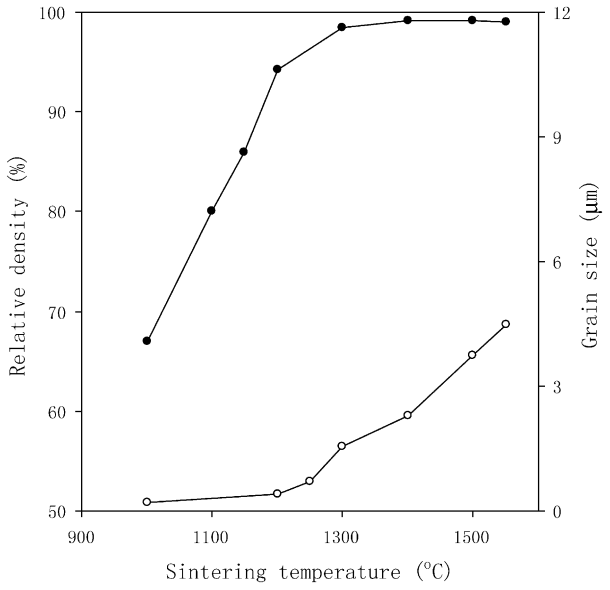

Fig. 3. The sintered density (•) and grain size (○) of $Ce_{0.85}Y_{0.15}O_{2-\delta}$ ceramics sintered at different temperatures for 3 h. The relative density of sintered samples is calculated using the theoretical density of 6.82 g/cm^3 that is obtained from Eq. (3).

$$\boldsymbol{d}_{\mathrm{th}} = \frac{4}{N_A a^3}\left[(1-x)M_{\mathrm{Ce}} + xM_{\mathrm{Y}} + \left(2-\frac{1}{2}x\right)M_{\mathrm{o}}\right] \qquad (3)$$

where $x=0.15$, a is the lattice constant of the solid solution at room temperature ($a=0.5403$ nm in this study based on XRD analysis), N_A is the Avogadro number, and M refers to the atomic weight. This yields $d_{\mathrm{th}}=6.82$ g/cm^3.

Fig. 3 shows the effect of sintering temperature for 3h on the density and grain size of $Ce_{0.85}Y_{0.15}O_{2-\delta}$ ceramics. We can see that the major densification has been completed with on significant grain growth in the temperature range of 1000–1200 °C. The $Ce_{0.85}Y_{0.15}O_{2-\delta}$ ceramic sintered at 1200 °C for 3 h has over 94.0% relative density, and a mean grain size of ~0.7 μm. Above 1200 °C, a rapid grain growth is observed. The sample sintered at 1300 °C for 3 h has over 98.5% relative density, and a mean grain size of ~1.55 μm. In the present study, this sample was chosen for the electrical and mechanical measurements.

The microsructural evolution of $Ce_{0.85}Y_{0.15}O_{2-\delta}$ ceramics in sintering temperature range of 1100–1550 °C is shown in Fig. 4. At all the temperatures used, no intragranular pores are observed, and all the pores are located at the grain boundaries or at the triple points. At 1100 °C (Fig. 4a), the pores exist in the form of continuous open porosity and exhibit a fair uniform distribution. With increasing the sintering temperature, pores are reduced in both the number and size. When the sintering temperatures are higher than 1300 °C, nearly all the pores are eliminated from the sintered bodies as shown in Fig. 4e.

3.3. Electrical properties

The ionic conductivity was measured by a two-probe impedance spectroscopy. The interpretation of impedance data for polycrystalline materials, such as yttria-stabilized zirconia, has been well documented.[26,27] Fig. 5 shows selected impedance plots measured at 350, 400, and 450 °C in air, respectively of the $Ce_{0.8}Gd_{0.2}O_{2-\delta}$ ceramic sintered at 1300 °C. The grain boundary, grain interior effects, and electrode polarization behavior can be clearly identified from these impedance plots. The quantitative change in GI and GB conductivities can be obtained by fitting these impedance plots using a software package, and the results are shown in Figs. 6 and 7.

Fig. 6 shows the temperature dependence of the GB conductivity to the total conductivity. As expected, the GB conductivity decreases as temperature decreases. However, it is interesting to note that above 300 °C, the GB conductivity is higher than GI one. At 500 °C, only ~24% of the total conductivity results from the GB effect. It is widely accepted that the predominate constituent of the grain boundary impurities in ceria-based solutions is SiO_2, and SiO_2 contamination results mainly from precursor chemicals and sample preparation.[28,29] An amorphous thin SiO_2 film will be formed between grains during sintering, blocking the movement of oxygen ions through grain boundary. This leads to a lower GB conductivity. At the present stage, however, the exact content of SiO_2 in the $Ce_{0.85}Y_{0.15}O_{2-\delta}$ ceramic is unavailable. High purity of raw chemicals used in this study should be a major reason that leads to a higher GB conductivity. Moreover, the higher sintered density and uniform microstructure as shown in Fig. 4d should also be beneficial for the GB conductivity.

From the Arrhenius plot in Fig. 7, the activation energies of around 0.895, 1.04, and 0.856 eV, respectively are obtained for total (E_t), grain boundary (E_{gb}), and grain interior (E_{gi}) conductivities. The total conductivity reaches ~4.59 $(\Omega m)^{-1}$ at 750 °C. The above results obtained in this study agree well with literature data from the samples sintered above 1400 °C, as listed in Table 1.[7–11]

3.4. Mechanical properties

Materials used in SOFC systems may be susceptible to fracture due to thermal stresses and mechanical stresses during cell fabrication and operation. However, unfortunately, ceria-based materials have very poor mechanical strength. It is expected that the mechanical properties can be improved by controlling grain size. The fracture toughness vs. crack size is first examined based on the equation as follows:[30]

$$K_{\mathrm{IC}} = 0.016\left(\frac{E}{H_{\mathrm{v}}}\right)^{1/2}\frac{P}{C^{3/2}} \qquad (4)$$

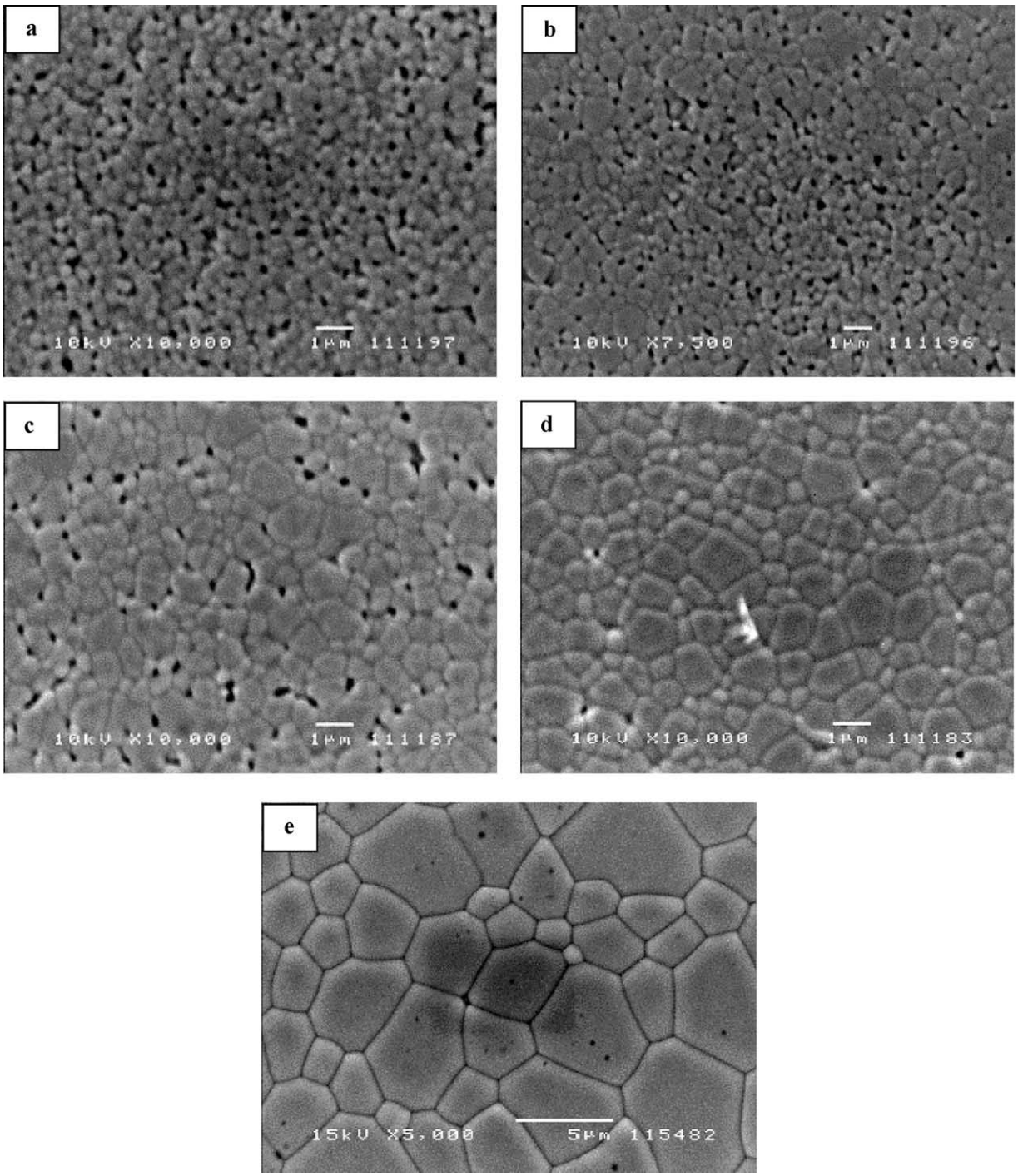

Fig. 4. SEM micrographs of $Ce_{0.85}Y_{0.15}O_{2-\delta}$ ceramics sintered at 1100 °C (a), 1150 °C (b), 1200 °C (c), 1300 °C (d), and 1550 °C (e) for 3 h.

where K_{IC} is fracture toughness, E is Young's modulus (205 GPa for Gd-doped ceria solid solutions[31]), H_v is Vickers hardness, P is the load and C is the half crack size. There are many indentation equations for the calculation of K_{IC} as presented in an extensive review by Ponton and Rawlings.[32] However, there are specific conditions and limitations for using these formulae because some of them are related to the treatment of indentation data based on a median crack and the other based on a Palmqvist crack. Moreover, some of these are suitable for certain materials; up to now no universal formula is available to evaluate the values of K_{IC} for all ceramic materials. For convenience, the above equation is selected in this study since this equation was used by Sammes et al.[33] and Shemilt et al.[34] for dealing with the indentation data of doped ceria-based ceramics. Moreover, as shown in Fig. 8, both the microhardness and the indentation fracture toughness are

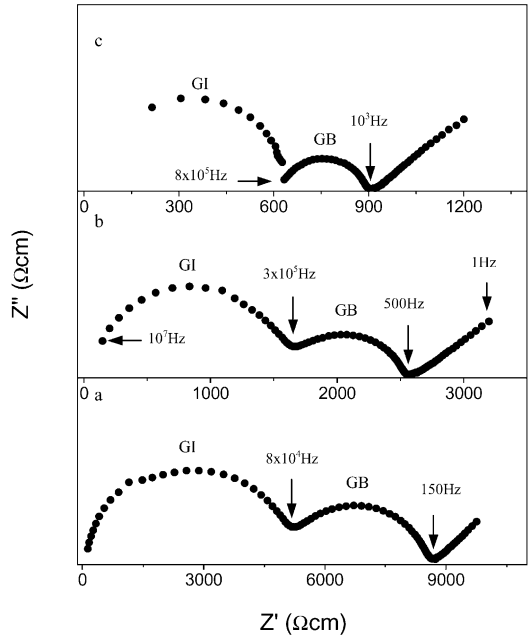

Fig. 5. Impedance plots of the $Ce_{0.85}Y_{0.15}O_{2-\delta}$ ceramic sintered at 1300°C for 3 h, measured at 350 °C (a), 400 °C (b), and 450 °C (c) in air. The GI and GB stand for grain interior and grain boundary effects, respectively.

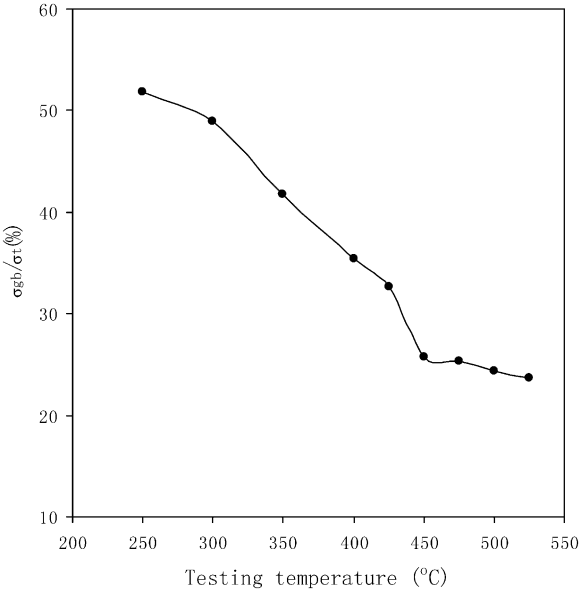

Fig. 6. The relative contribution of the grain boundary conductivity (σ_{gb}) to the total conductivity (σ_t) of the $Ce_{0.85}Y_{0.15}O_{2-\delta}$ ceramic sintered at 1300 °C for 3 h.

independent of crack length. SEM observation indicates that the indentation cracks propagate in the transgranular fracture mode for all the samples used. This is a typical characteristic for the materials with cubic structure.

Table 3 lists the selected literature data, together with our results regarding the fracture toughness of ceria-based ceramics. It can be seen that the values of fracture

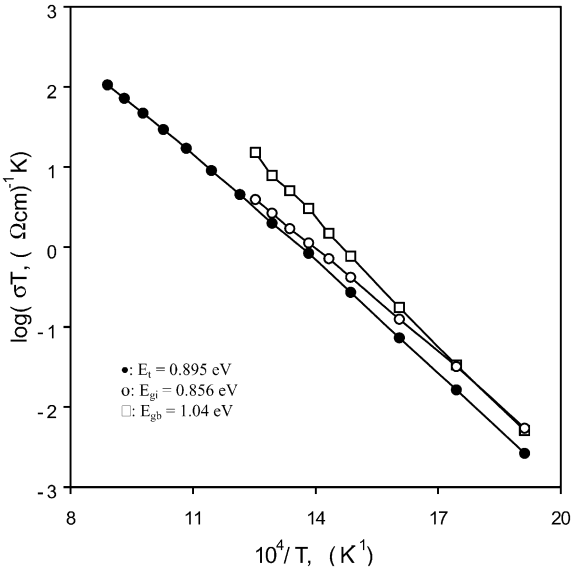

Fig. 7. Arrhenus plots of the total (•), GI (○), and GB (□) conductivities of the $Ce_{0.85}Y_{0.15}O_{2-\delta}$ ceramics sintered at 1300°c for 3 h. E_t, E_{gi}, and E_{gb} respectively stand for the activation energies for the total, GI, and GB conductivities.

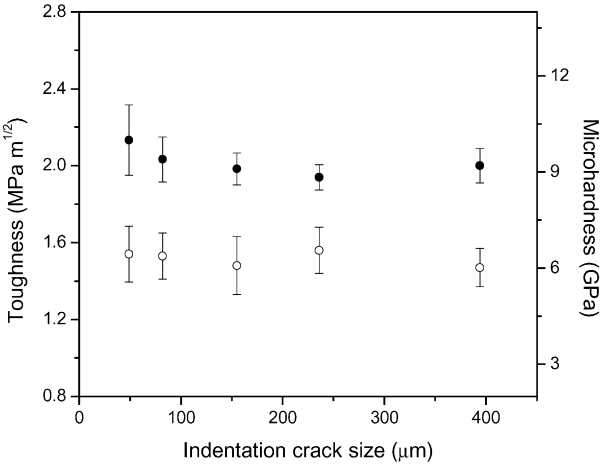

Fig. 8. Fracture toughness (○) and microhardness (•), respectively vs. indentation crack size for the $Ce_{0.85}Y_{0.15}O_{2-\delta}$ ceramic sintered at 1300 °C for 3 h.

toughness, K_{IC}, are somewhat scattering, depending on testing methods and investigators.[33–35] Basically, the K_{IC} values (Table 3) of these ceria ceramics are at the lower end of the range (1.5–4.2 MPa $m^{1/2}$) for fully stabilized zirconias[36,37] and significantly lower than those of partially stabilized zirconias. Moreover, the fracture toughness of cerias seems insensitive to types of dopants and dopant concentration. On the other hand, according to Ponton and Rawlings,[32] the measured toughness values should rank as SENB K_{IC} > actual K_{IC} > indentation K_{IC}. However, it is interesting to note that the indentation K_{IC} by Sammes et al.[33] and by Shemilt et al.[34] is much higher than that obtained by SENB method. But our values are fairly close to the

Table 3
Selected literature data, together with our results regarding the fracture toughness of ceria-based ceramics

Composition	Density (%)	Grain size (μm)	Testing method	Fracture toughness K_{IC} (MPa $m^{1/2}$)	Ref.
CeO_2	94	3.5	SENB[a]	1.5	35
$(Ce_{0.8}Zr_{0.2})O_2$	94.5	3.5	SENB	1.6	35
$(Ce_{0.9}Sm_{0.1})O_{2-\delta}$	96		Indentation[b]	2.4±0.3	34
$(Ce_{0.8}Sm_{0.2})O_{2-\delta}$	94		Indentation	2.4±0.3	34
$(Ce_{0.9}Sm_{0.1})O_{2-\delta}$	96		SENB	1.28±0.15	34
$(Ce_{0.8}Gd_{0.2})O_{2-\delta}$	95		Indentation	2.08±0.31	33
$(Ce_{0.85}Y_{0.15})O_{2-\delta}$	97.0	0.87	Indentation	1.50±0.20	This study
$(Ce_{0.85}Y_{0.15})O_{2-\delta}$	98.5	1.55	Indentation	1.49±0.20	This study
$(Ce_{0.85}Y_{0.15})O_{2-\delta}$	99.2	4.52	Indentation	1.53±0.20	This study

[a] Single edge notched bend.
[b] All the indentation K_{IC} here calculated based on Eq. (4).

SENB K_{IC} by Shemilt et al.[34] as shown in Table 3. The difference may be mainly resulted from the measurement errors on the length of indentation cracks. The end point of indentation cracks for ceria-based ceramics cannot be easily identified under ordinary microscope due to poor resolution. In our case, the length of indentation cracks was accurately measured under SEM.

It also should be pointed out based on Table 3 that no significant dependence of fracture toughness on grain size is found in this study. This indicates that the mechanical stability of ceria-based ceramics cannot be obtained by just controlling grain size.

4. Conclusions

The coprecipitated powder calcined at 700 °C for 3 h has an optimal sinterability. The major densification has been completed with on significant grain growth in the temperature range of 1000 to 1200 °C. The sample sintered at 1200 °C for 3 h has over 94.0% relative density, and a mean grain size of ~0.7 μm. Above 1300 °C, almost fully dense $Ce_{0.85}Y_{0.15}O_{2-\delta}$ ceramics can be obtained in 3 h.

The $Ce_{0.85}Y_{0.15}O_{2-\delta}$ ceramic sintered at 1300 °C in 3 h has a higher ionic conductivity [4.59 $(\Omega m)^{-1}$ at 750 °C in air]. At 500 °C, only ~24% of the total conductivity results from grain boundary effect. The activation energies of ~0.895, 1.04, and 0.856 eV, respectively are obtained for total (E_t), grain boundary (E_{gb}), and grain interior (E_{gi}) conductivities.

Both the microhardness and fracture toughness are independent of crack length. The indentation cracks propagate in the transgranular fracture mode for all the samples used. No significant dependence of fracture toughness on grain size is found for the dense $Ce_{0.85}Y_{0.15}O_{2-\delta}$ ceramics, indicating that the mechanical stability cannot be improved by controlling grain size.

References

1. Blumenthal, R. N., Brugner, F. S. and Garnier, J. E., *J. Electrochem. Soc.*, 1973, **120**, 1230.
2. Yahiro, H., Eguchi, K. and Arai, H., *Solid State Ionics*, 1986, **21**, 37.
3. Faber, J., Geoffroy, C., Roux, A., Sylvestre, A. and Abelard, P., *Appl. Phys. A*, 1989, **49**, 225.
4. Balazs, G. B. and Glass, R. S., *Solid State Ionics*, 1995, **76**, 155.
5. Gerhard-Anderson, R. and Nowick, A. S., *Solid State Ionics*, 1981, **5**, 547.
6. Kilner, J. A., *Solid State Ionics*, 1983, **8**, 201.
7. Dirstine, R. T., Blumenthal, R. N. and Kuech, T. F., *J. Electrochem. Soc.*, 1979, **126**, 264.
8. Wang, D. Y. and Nowick, A. S., *J. Solid State Chem.*, 1980, **35**, 325.
9. Pascual, C., Jurado, J. R., Arroyo, G. F., Del Olmo, L., Moure, C. and Duran, P., *Science of Ceramics*, 1984, **12**, 729.
10. Yahiro, H., Baba, Y., Eguchi, K. and Arai, H., *J. Electrochem. Soc.*, 1988, **135**, 2077.
11. Herle, J. V., Horita, T., Kawada, T., Sakai, N., Yokoawa, H. and Dokiya, M., *J. Eur. Ceram. Soc.*, 1996, **16**, 961.
12. Eguchi, K., Setoguchi, T., Inone, T. and Arai, H., *Solid State Ionics*, 1992, **52**, 165.
13. Zhang, T. S., Hing, P., Huang, H. and Kilner, J. A., *Solid State Ionics*, 2002, **148**, 567.
14. Hohnke, D. K., *Solid State Ionics*, 1981, **5**, 531.
15. Kudo, T. and Obayashi, H., *J. Electrochem. Soc.*, 1975, **122**, 142.
16. Zhang, T. S., Ma, J., Kong, L. B., Hing, P. and Kilner, J. A., *Solid State Ionics* (in preparation).
17. Chiang, Y. M., Lavik, E. B. and Blom, D. A., *Nanostruct. Mater.*, 1997, **9**, 633.
18. Chiang, Y. M., Lavik, E. B., Osack, I. K., Tuller, H. L. and Ying, J. M., *J. Electroceram.*, 1997, **1**, 7.
19. Kirk, T. J. and Winnick, J., *J. Electrochem. Soc.*, 1993, **140**, 3494.
20. Higashi, K., Sonada, K., Ono, H., Sameshima, S. and Hirata, Y. H., *J. Mater. Res.*, 1999, **14**, 957.
21. Briois, V., Williams, C. E., Dexpert, H., Villain, F., Cabane, B., Deneuve, F. and Magnier, C., *J. Mater. Sci.*, 1993, **28**, 5019.
22. Chu, X., Chung, W. and Schmidt, L. D., *J. Am. Ceram. Soc.*, 1993, **76**, 2115.
23. Chen, P. L. and Chen, I. W., *J. Am. Ceram. Soc.*, 1993, **76**, 1577.
24. Klug, H. P. and Alexaander, L. E., *X-ray Diffraction Procedures*. Wiley, New York, 1954 (Chapter 9).
25. Riess, I., Braunshtein, D. and Tannhauser, D. S., *J. Am. Ceram. Soc.*, 1981, **64**, 479.
26. Bauerle, J. E., *J. Phys. Chem. Solids*, 1969, **30**, 2651.

27. Macdonald, J. R., ed., *Impedance Spectroscopy—Emphasizing Solid Materials and Systems*. A Wiley-Interscience Publication, John Wiley & Sons, 1987.
28. Steele, B. C. H., *Solid State Ionics*, 2000, **129**, 95.
29. Gerhardt, R., Nowick, A. S., Mochel, M. E. and Dumiler, I., *J. Am. Ceram. Soc*., 1986, **69**, 647.
30. Anstis, G. R., Chantikul, P., Lawn, B. R. and Marshall, D. B., *J. Am. Ceram. Soc*., 1981, **64**, 533.
31. Argoitia, A., Baumard, J. F. and Gault, C. In *High Tech. Ceram*., ed. P. Vincenzini. Elsevier Science, Amsterdam, 1987.
32. Poton, B. C. and Rawlings, R. D., *Mater. Sci. Tech*., 1989, **5**, 865.
33. Sammes, N. M. and Zhang, Y. In *Proc. Sec. Europ. SOFC Forum, Vol. 2*, ed. B. Thotstensen. Oberrohrdorf, Switzerland, 1996. p. 697.
34. Shemilt, J. E., Williams, H. M., Edirisinghe, M. J., Evans, J. R. G. and Ralph, B. *Acta Metallurgica*, 1997, **36**, 929.
35. Mashina, S., Shaizero, O. and Meriani, S., *J. Eur. Ceram. Soc*., 1992, **9**, 127.
36. Jue, J. F. and Virkar, A. V., *J. Am. Ceram. Soc*., 1990, **73**, 3650.
37. Abraham, I. and Gritzer, G., *J. Eur. Ceram. Soc*., 1996, **71**, 16.